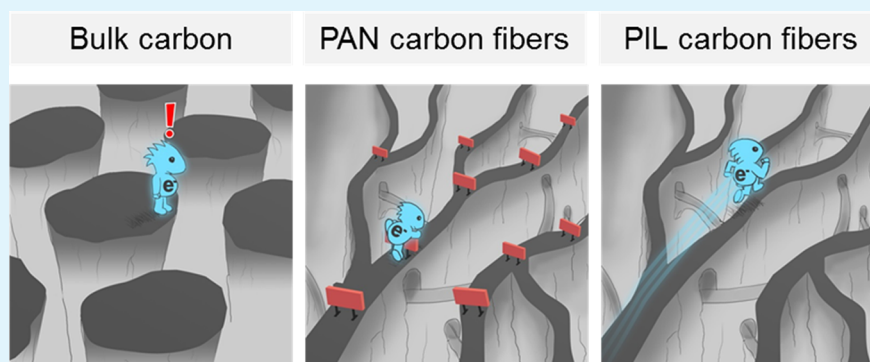


# Electrospun Carbon Fibers Replace Metals as a Current Collector in Supercapacitors

Elinor Josef,<sup>\*</sup> Runyu Yan, Ryan Guterman,<sup>†</sup> and Martin Oschatz

Department of Colloids Chemistry, Research Campus Golm, Max Planck Institute of Colloids and Interfaces, Am Mühlenberg 1, 14476 Potsdam, Germany

## Supporting Information



**ABSTRACT:** The final step toward a completely metal-free electrochemical energy device requires the replacement of the metal current collector with conductive carbon. This article describes the use of carbon fibers derived from electrospun poly(ionic liquid) as the current collector. Fibers were stabilized by ionic cross-linking with a small organic acid, followed by heating to 950 °C under N<sub>2</sub> to create a conductive and free-standing carbon fleece. The resultant carbon fibers were utilized as current collectors in EDLCs in both aqueous (1 M Na<sub>2</sub>SO<sub>4</sub> in water) and organic (1 M tetraethylammonium tetrafluoroborate in acetonitrile) electrolytes. In both cases, carbon fibers outperformed the established carbon-coated aluminum foil and showed performances comparable to platinum. They operated at current densities of up to 40 A g<sup>-1</sup> without significant signs of resistivity. We found that both the nanostructure resulting from spinning and the use of PIL as a carbon precursor are crucial in obtaining this performance. These carbon fibers are only 2–10% the weight of the aluminum current collector and thus increase the gravimetric energy density of the whole cell. PIL-derived carbon fibers could be a promising inexpensive and metal-free alternative for future electric double-layer capacitor applications.

**KEYWORDS:** carbon nanofibers, electric double-layer supercapacitors, metal-free, electrospinning, poly(ionic liquid)s, current collectors

## INTRODUCTION

Electric double-layer capacitors (EDLCs) are at the frontier of energy storage devices, with applications ranging from portable electronics to electrical vehicles.<sup>1–3</sup> In EDLCs that operate using aqueous or organic solvent-based electrolytes, charge storage takes place by the reversible electrosorption of electrolyte ions on the surface of a porous carbonaceous electrode material. Because of the absence of time-consuming redox processes and constantly changing physicochemical properties of the electrode materials that are present in batteries, EDLCs provide high power densities and nearly unlimited cycle life. Over the past 20 years, the majority of research efforts on EDLCs have focused on the enhancement of electroactive materials and understanding the charge storage mechanism in a given electrolyte system.<sup>4–9</sup> Less attention has been paid to current collectors (CCs) and their interface with the active material, despite their crucial influence on the overall energy storage performance of EDLCs.<sup>10–13</sup>

The role of CCs is to collect and transport electrons from and to the active materials. To effectively accomplish this, materials with high conductivity are required, such as aluminum, copper, or stainless steel. While these metals are mechanically robust and free-standing, they often corrode in non-neutral aqueous electrolyte, and their heavy weight decreases the gravimetric energy density of the whole cell. In addition, the interfacial resistance between the metal CC and the carbon electrode contributes to the internal resistance of the EDLC and limits its power capability.<sup>14</sup> To overcome the interfacial resistance, metals can be coated with carbon, which has led to the wide use of carbon-coated aluminum foil CCs in EDLCs. Replacing the metal CC with one composed of carbon materials could rectify the issues associated with metal CCs

Received: May 1, 2019

Accepted: July 9, 2019

Published: July 9, 2019

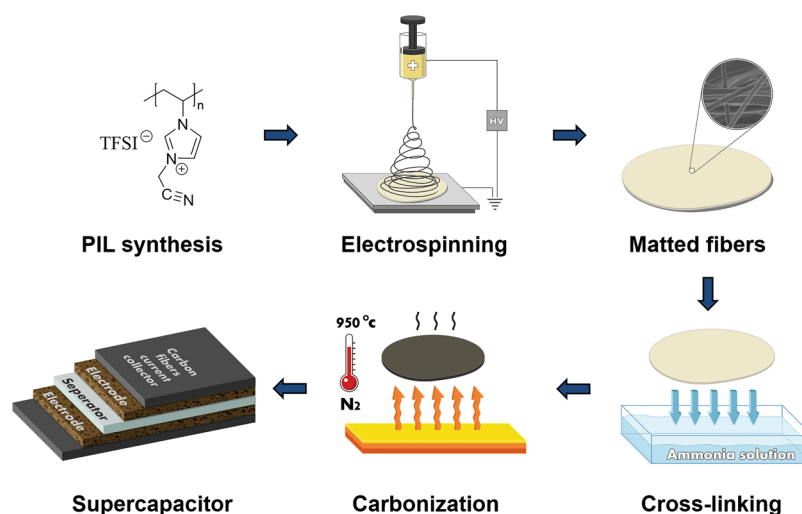


**Figure 1.** Process scheme for the production of PIL-derived carbon current collector. PIL was synthesized and then electrospun in a solution containing an organic acid as a cross-linker. The resultant matted fibers were immersed in ammonia solution for cross-linking and dried. Fibers were carbonized under  $N_2$  at  $950\text{ }^\circ\text{C}$  and utilized in EDLC as the current collector instead of a metal.

and also be the final step to completely metal-free electrochemical energy storage devices.<sup>15,16</sup> In contrast to conventional metallic or metal-supported CCs, carbon-based materials also provide the possibility of fabricating flexible electrodes.<sup>17,18</sup> Replacing the metal CCs in batteries and supercapacitors with carbons has been attempted with carbon nanotubes (CNT),<sup>11,19–25</sup> carbon cloth,<sup>26</sup> graphite foil,<sup>15,27</sup> graphene reinforced with PANI carbon fibers,<sup>17</sup> graphitized carbon fibers, and non-graphitic PAN carbon fibers.<sup>28</sup> However, there is still a need to produce a carbon CC in a scalable method with sufficient conductivity for high scan rates in supercapacitors. To the best of our knowledge this is yet to be achieved.

To accomplish carbon CCs, the carbon should ideally possess a continuous structure with minimum interface effects to improve conductivity, while also provide an intimate contact with the active species of the electrode. One-dimensional fiber-type carbon materials are particularly promising for this purpose<sup>29</sup> and can be produced by using different methods such as chemical vapor deposition, melt spinning, and electrospinning.<sup>30</sup> Among these, electrospinning stands out as a scalable and inexpensive technique to produce continuous fibers with diameters from tenths of nanometers to a few micrometers, having a defined architecture and high surface area.<sup>29,31</sup> While micrometer-sized carbon fibers as the ones in commercial carbon cloth are produced using mesophase pitch or PAN as precursor,<sup>32</sup> electrospinning is more versatile in the choice of materials and can thus grant additional functions to the resultant carbon nanofibers. In addition, electrospun carbon fibers can form a free-standing sheet; a continuous structure that can be incorporated into macroscopic devices is more difficult to achieve with carbon nanotubes. While electrospinning is a widely used method for the fabrication of active electrode materials<sup>33–35</sup> and for the immobilization of electroactive oxides at high areal loading,<sup>36</sup> to date it has not been coupled to porous carbon electrode materials to fabricate CCs for classical EDLCs with purely capacitive charge storage mechanism. The engineering of such materials with one-dimensional architecture in symmetric two-electrode devices remains a particular challenge. CCs require low electronic resistance, which is typically too high for polymer-derived

carbon,<sup>37</sup> even when supplemented with more conductive materials such as pitch,<sup>38</sup> carbon nanotubes,<sup>39</sup> graphene,<sup>40,41</sup> and metallic nanoparticles.<sup>42</sup> This roadblock may be overcome by the development of new spinnable polymers that yield more conductive carbons.

Poly(ionic liquid)s (PILs) are a class of polymers composed of ionic liquid monomers<sup>43–48</sup> and are promising candidates to produce carbons that are more conductive compared to established nonionic precursors.<sup>49,50</sup> The use of ionic liquids as carbon precursors is a relatively new method for the synthesis of carbon materials,<sup>51</sup> but it is gaining increasing interest also because it is an efficient route to produce heteroatom-doped carbons in high yields without postcarbonization processes.<sup>52</sup> Doping carbons with heteroatoms can increase the electric conductivity and catalytic activity compared to pristine carbon; nitrogen-doped carbon in particular is intensely investigated.<sup>53,54</sup> Polymerized ionic liquids, i.e., PILs, combine the carbon properties of ionic liquids with the processability and mechanical stability of polymers. While carbonization of ionic liquids themselves leads to carbon in powder form, PILs have the potential of forming free-standing carbons with different geometrical structures such as fibers. Carbon nanofibers derived from PILs could thus be more conductive than other carbons as a result of a synergistic effect of high electric conductivity of the carbon itself (enhanced by heteroatom doping) and a continuous structure that allows efficient transport of electrons by minimizing interface effects. PILs, like other polyelectrolytes, can be challenging to electrospin due to their high conductivity and the low mobility of the polyion, causing instabilities in the electrospinning jet.<sup>55</sup> While a few groups have electrospun PILs,<sup>50,56–59</sup> any attempt to carbonize the fibers resulted in complete loss of structure<sup>50</sup> or a carbon too brittle to measure its impedance.<sup>56</sup>

In this context, we developed conductive carbon fibers from PIL as current collectors in EDLCs. A schematic illustration for the preparation of carbonized PIL fibers is shown in Figure 1. PIL fibers were produced by electrospinning followed by a critical cross-linking step to preserve the fiber structure after carbonization. The cross-linking step was accomplished by including a multifunctional organic acid in the spinning solution, and a postspinning treatment with base, which

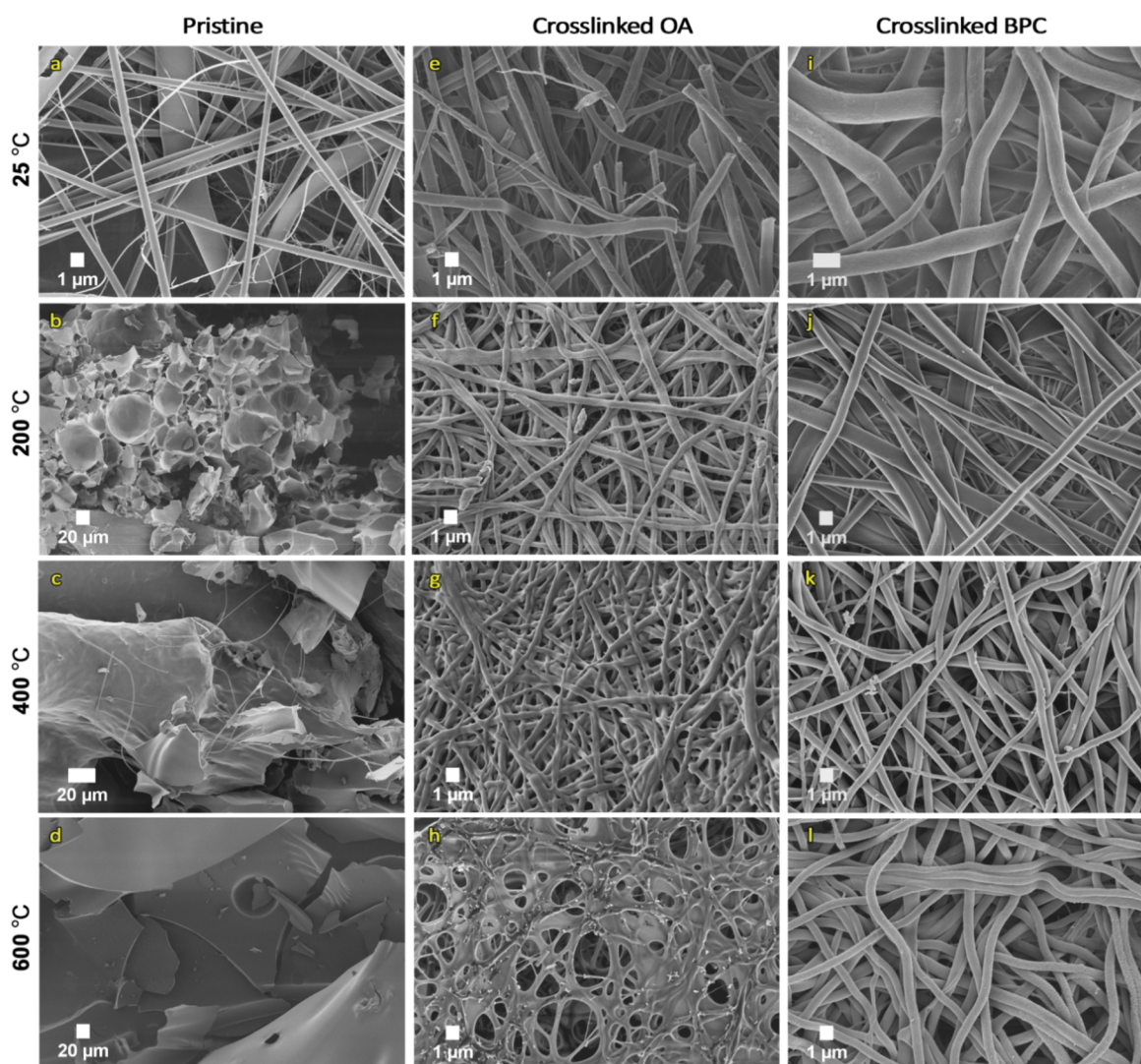


**Figure 2.** SEM micrographs of fibers spun with OA (a–h) and BPC (i–l) as a cross-linker, without (a–d) and with (e–l) cross-linking. Pictures (a, e, i) are at room temperature, either pristine (a) or after cross-linking (e, i). Fibers were subsequently heated under  $N_2$  to temperatures of 200 °C (b, f, j), 400 °C (c, g, k), and 600 °C (d, h, l).

induced ionic cross-linking between the PIL and organic acid. Cross-linked fibers were carbonized at 950 °C and used as current collectors in EDLCs using aqueous or organic electrolytes. EDLCs devices based on carbonized PIL fibers show comparable energy storage properties to devices with platinum foil as the current collector. They can be operated at current densities of up to 40  $A\ g^{-1}$  without significant loss of capacity. In contrast, those EDLCs using carbon-coated aluminum foil, nonspun PIL-derived carbon film, or polyacrylonitrile-derived carbon fibers fail to operate under such conditions. This shows the synergistic effect between the one-dimensional nanostructure and the high conductivity of the carbonized PIL fibers and is a step toward all carbon, flexible, and lightweight EDLCs.

## RESULTS AND DISCUSSION

Poly(3-cyanomethyl-1-vinylimidazolium bis(trifluoromethanesulfonyl)imide) (PIL) was synthesized according to a literature procedure.<sup>60</sup> It was then electrospun from a solution containing 20 wt % PIL with 5 wt % polyvinylpyrrolidone (PVP) as the supporting polymer in a mixture of DMF and

methanol (25:75 weight ratio). PVP is often used in electrospinning as a blending polymer due to its solubility in water and organic solvents and its electrospinnability.<sup>59</sup> Using bis(trifluoromethanesulfonyl)imide (TFSI) as the counterion promoted the solubility of PIL in polar organic solvents, which are more easy to electrospin compared to aqueous solutions. A mixture of solvents was crucial for electrospinning; DMF alone failed to produce fibers, while methanol did not solubilize the required concentration of PIL. Once fibers were produced, we attempted to carbonize them, but the structure was destroyed. Retaining the structure of fibers during carbonization can be achieved by cross-linking the polymers.<sup>61</sup> Because cross-linked polymers are not soluble and thus not spinnable, the cross-linking step must occur after PIL fiber formation. Many cross-linking methodologies been achieved for PILs, including chemical<sup>62</sup> and physical<sup>63–65</sup> routes. In particular, Zhao et al.<sup>64</sup> mixed small organic acids with PILs in a solvent, which underwent ionic cross-linking upon the introduction of base. The acids were immediately deprotonated by excessive  $NH_3$  into carboxylate anions, followed by complexation with the cationic PIL to create ionic cross-links. Similarly, Täuber et al. showed that this cross-linking step can occur in solid PIL films,

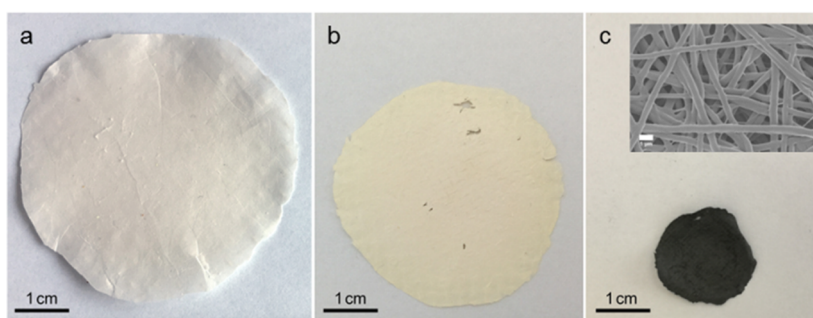


**Figure 3.** Digital photographs of a collected sheet in different steps: pristine (a), cross-linked (b), and carbonized at 950 °C (c). The inset in (c) is the SEM micrograph of the carbonized sheet. Fibers were spun with BPC as a cross-linker.

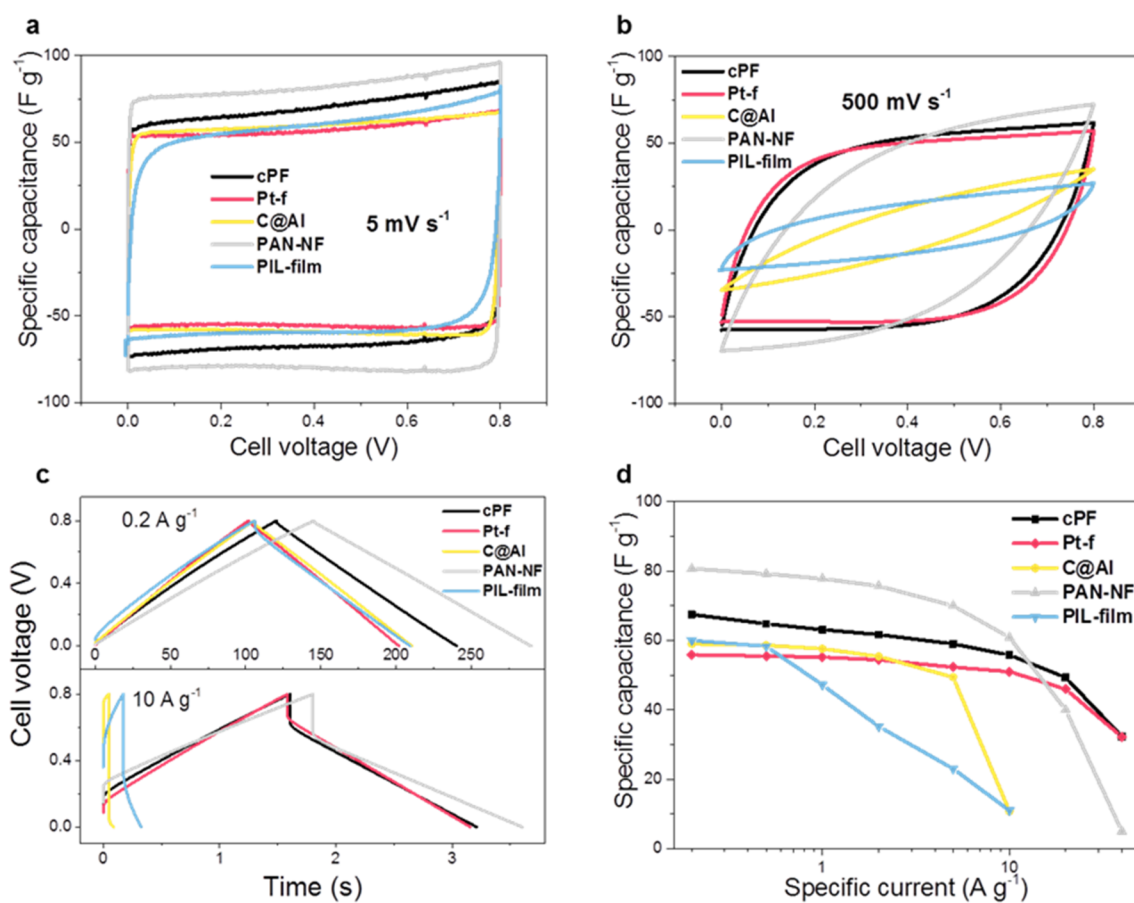


**Figure 4.** Cyclic voltammograms at scan rates of 5 (a) and 500  $\text{mV s}^{-1}$  (b), charge–discharge curves at current densities of 0.2 and 10  $\text{A g}^{-1}$  (c), and specific capacitance at different current densities (d) of symmetric supercapacitors with Ketjen black carbon as the electrodes and 1 M  $\text{Na}_2\text{SO}_4$  aqueous electrolyte. Carbonized PIL fibers (cPF), platinum foil (Pt-f), carbon-coated aluminum foil (C@Al), carbonized PAN fibers (PAN-NF), and PIL in film form (PIL-film) were used as the current collectors.

thus demonstrating a viable and convenient route for cross-linking after casting of a PIL.<sup>65</sup> We postulated that this method could be applied to stabilize the fiber structure by first spinning PIL solutions containing organic acids and then exposing the fibers to an ammonia solution to facilitate cross-linking. We examined two acids, benzenepentacarboxylic acid (BPC) and oxalic acid (OA), as potential cross-linkers. Details on the optimization of cross-linker concentrations can be found in the [Supporting Information](#). After spinning, we immersed the fibers in aqueous ammonia to ionically cross-link the PIL. SEM micrographs of the fibers show that the structure remained intact after the complexation step (Figure 2e,i). Without cross-linking, the fibers dissolved in methanol instantly, whereas after

cross-linking they did not. To test the stability of the fibers against heating, fibers with OA (cross-linked and non-cross-linked) and BPC were carbonized at 200, 400, and 600 °C (Figure 2). We found that without the cross-linking step there was loss of the fiber structure at 200 °C due to polymer plasticization, while for the cross-linked materials there was no such structure deformation, illustrating the importance of ionically cross-linking the PIL to retain fiber integrity. The type of cross-linker also had a pronounced effect on the integrity of the fibers. Cross-linker OA barely maintained the fiber structure up to 400 °C (Figure 2g), while at 600 °C fiber structure was completely lost (Figure 2h). By use of BPC, however, carbon fibers were retained even at 600 °C (Figure

2i), indicating more effective cross-linking as compared to OA. We found that the resistance of this carbon was still quite high but could be reduced if carbonized at 950 °C (hereafter termed carbonized PIL fibers (cPF), Figure S1a), making this material the best candidate for testing in EDLC. To the best of our knowledge, this is the first example of a successful carbonization of electrospun PIL fibers.

To fabricate a carbon of sufficient size for use in an EDLC, a polymer fleece ~5 cm in diameter was prepared, immersed in  $\text{NH}_3(\text{aq})$ , and then carbonized at 950 °C (Figure 3). Both the cross-linking step and carbonization resulted in shrinkage of the material, which can be explained by first a reduction in free volume by the cross-linking step and then mass loss after carbonization (carbonization yield was found to be 15.6%; Figure S2). Elemental analysis shows that cPF had nitrogen content of 8 wt % (Table S1), similar to a PIL membrane<sup>66</sup> and other carbonized PILs.<sup>50</sup>

Studies suggest that carbon doped with a low amount of nitrogen can have a higher conductivity compared to undoped carbon.<sup>56,67</sup>

The one-dimensional nanoarchitecture and potential high conductivity of cPF render them as promising current collectors in EDLCs. To assess the potential of these fibers, they were compared to a series of reference CCs. Platinum foil (Pt-f) typically performs excellently as a CC because of its high corrosion resistance and outstanding conductivity, but its high price hinders commercial application. We chose carbon-coated aluminum (C@Al) as another reference since it is the commercial standard CC for EDLCs. Nonspun PIL-derived bulk carbon prepared in a film form (PIL-film) and polyacrylonitrile-derived carbon fibers (PAN-NF) were tested, too, to determine whether the performance of the PIL-derived carbon fibers stems from the PIL itself, the nanoarchitecture, or their combination. For the electrode, commercial Ketjen black carbon was used as the active material. Because of its open pore structure, high electrical conductivity, and high specific surface area, Ketjen black has been used as an active material in electrodes of ultrafast supercapacitors.<sup>68–70</sup> Because of its high conductivity, Ketjen black imposes high demands on the conductivity of CC and was thus chosen as a standard for comparing the performance of different CCs and testing their conductivity limits. The nitrogen physisorption isotherms and pore size distributions of Ketjen black (Figure S10) show the presence of abundant micropores and broadly distributed mesopores with diameters in the range 3–30 nm. In principle, the micropores provide more adsorption sites for a higher capacitance, while the mesopores can facilitate the ion transport for a better rate capability.<sup>71</sup>

Cyclic voltammetry (CV) measurements of an EDLC operating in 1 M  $\text{Na}_2\text{SO}_4$  aqueous electrolyte with a sheet of cPF as the CC show nearly ideal capacitive behavior of cPF. At a low scan rate of 5  $\text{mV s}^{-1}$ , the curve of cPF was rectangular, indicating purely capacitive energy storage behavior as typically observed for EDLCs (Figure 4a). Already at a low scan rate of 5  $\text{mV s}^{-1}$ , the CV curve of PIL-film deviated from the perfectly rectangular shape, indicating a higher charge transfer resistance when this material is applied as CC. This underlines the beneficial effect of one-dimensional nanostructuring of PIL-derived carbons for efficient charge transfer. At a high scan rate of 500  $\text{mV s}^{-1}$  (Figure 4b), the CVs of the devices operated with PIL-film, PAN-NF, and C@Al deviated more significantly from the rectangular shape than Pt-f and the cPF CCs, indicating that the latter have comparable charge-transfer

properties. Charge–discharge curves (Figure 4c) show a symmetric triangle shape at the lowest current density of 0.2  $\text{A g}^{-1}$ . This is the anticipated curve for an EDLC, consistent with the CV data. At a high specific current of 10  $\text{A g}^{-1}$ , PIL-film and C@Al lost the triangle shape, signifying the high resistance in those devices. Under the same conditions, cPF had a triangular shape similar to Pt-f, and both showed the smallest voltage drop due to low internal resistance. The specific capacitance was analyzed over a current density range from 0.2 to 40  $\text{A g}^{-1}$  (Figure 4d). cPF had a high-power behavior comparable to Pt-f, whereas other CCs showed a significant drop. Accordingly, the impedance of cPF was nearly similar to platinum, observed by the vertical shape in low frequency range of Nyquist plot, whereas all other CCs tested showed higher resistances (Figure S3). The Nyquist plots have been fitted according the equivalent circuit.<sup>72</sup> The results indicate that the main differences among different current collectors are the  $R_s$  and  $R_{ct}$ . Basically, the intrinsic ohmic resistance  $R_s$  mainly originates from the intrinsic resistances of electrode material, electrolyte, current collector, and separator. The interfacial charge transfer resistance  $R_{ct}$  (the diameter of the semicircle) mainly comes from the electronic and ionic resistances at the interfaces, in addition to the ion and electron conductivity of the whole system.<sup>73</sup> Therefore, the low  $R_s$  of cPF indicates the low intrinsic resistance, which is attributed to its high electric conductivity. The low  $R_{ct}$  of cPF reveals the low resistance of the interfaces, which could be due to the intimate interfacial contact between the electrode and the current collector. Thus, cPF is a metal-free carbon CC that demonstrates the same behavior as platinum and outperforms the chosen reference CCs in an aqueous EDLC.

The surface area of cPF was measured by  $\text{N}_2$  physisorption and calculated to be 287  $\text{m}^2 \text{g}^{-1}$  by using multipoint BET analysis (Figure S4), while the surface area of PAN-NF and PIL-film was found to be 10 and 24  $\text{m}^2 \text{g}^{-1}$ , respectively. To test whether the high surface area of the cPF is the reason for the better performance as a current collector, another EDLC was assembled, where cPF functions as both the active material and the current collector, and no additional carbon electrode was used (i.e., the EDLC was composed of two cPF sheets and a separator). This EDLC had only a minor capacity (Figure S5); thus, it can be concluded that the contribution of the cPF current collector to the charge storage capacity remains low. However, it might account for the slightly higher capacitance at low scan rates of the EDLCs with cPFs as the current collector in comparison to the devices with Pt-f. An SEM image of cPF after cycling operation in the EDLC (1000 cycles at a specific current of 1  $\text{A g}^{-1}$ ) demonstrated no deterioration in the fibrous structure of cPF, underlining the stability of cPF during the EDLC measurements (Figure S11).

The sheet resistance of cPF and PAN-NF was measured by using a four-point probe. The resistance of cPF, 18  $\Omega \text{sq}^{-1}$ , was significantly lower than that of PAN-NF, 58  $\Omega \text{sq}^{-1}$  (Table S2). Therefore, the superior performance of cPF over PAN-NF as CC at high current densities and scan rates can be attributed to the lower resistance of the cPF. cPF and PAN-NF were further characterized by using X-ray diffraction (XRD) and Raman spectroscopy. XRD patterns exhibit broad peaks near 25° and 44°, which can be assigned to the (002) and (100) layers of graphitic crystallites (Figure S6a).<sup>74,75</sup> Raman spectra of the three samples show two bands near 1350  $\text{cm}^{-1}$  (D-band) and 1600  $\text{cm}^{-1}$  (G-band), which are typical for disordered graphitic-like materials (Figure S6b).<sup>76</sup> The D-

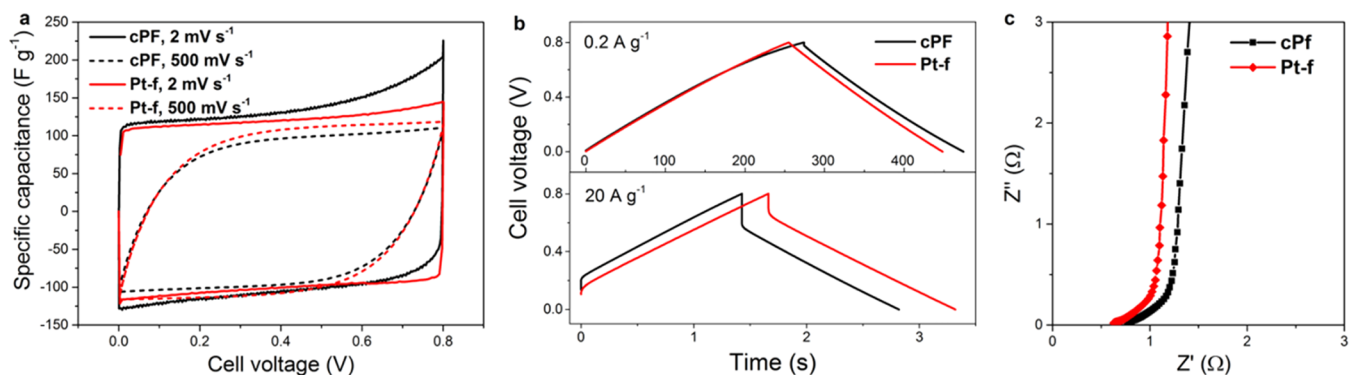


**Figure 5.** Cyclic voltammograms at scan rates of 2 and 500  $\text{mV s}^{-1}$  (a), charge–discharge curves at current densities of 0.2 and 20  $\text{A g}^{-1}$  (b), and impedance spectra (c) of EDLCs operated with 1 M  $\text{Na}_2\text{SO}_4$  aqueous electrolyte and in-house made HSTC electrodes. Carbonized PIL fibers (cPF) and platinum foil (Pt-f) were used as current collectors.

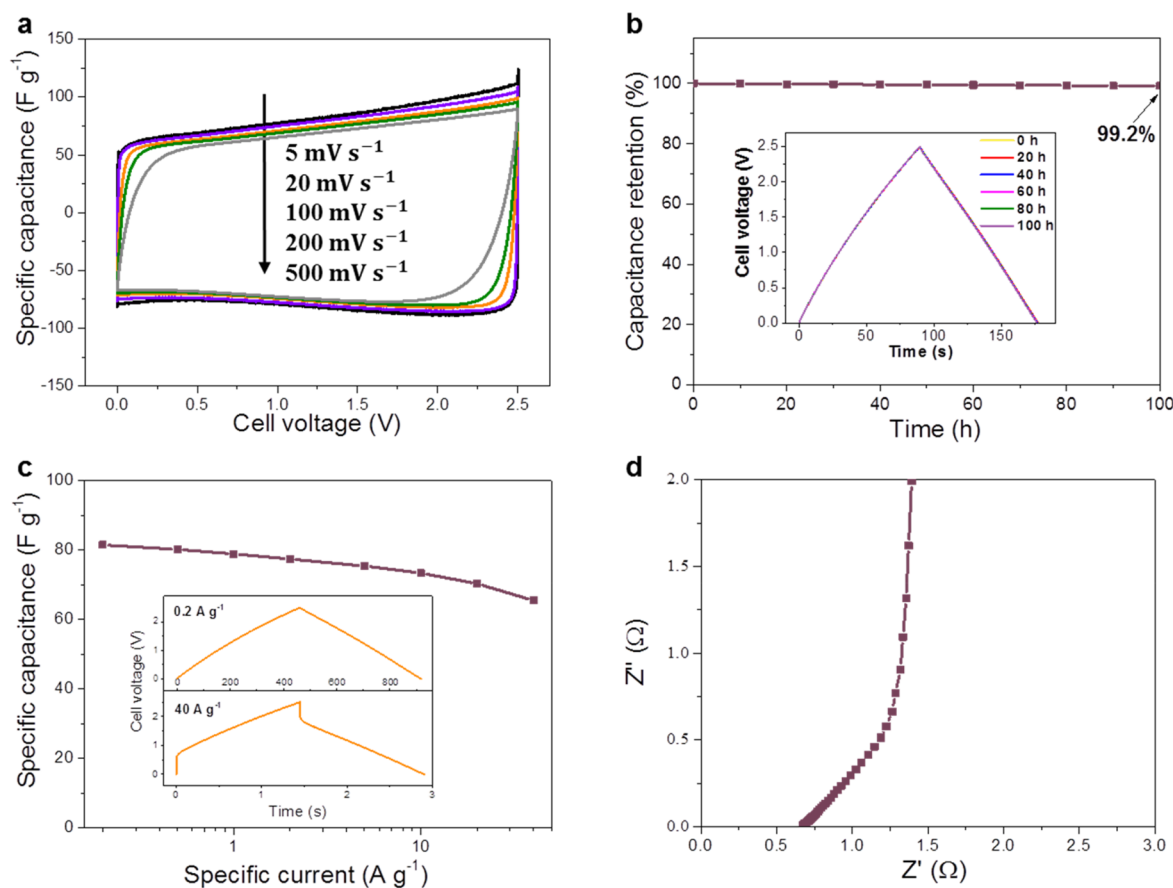


**Figure 6.** Cyclic voltammograms at different scan rates (a), voltage floating stability test (b), selected charge–discharge curves and specific capacitance at different specific currents (c), and impedance spectrum (d) of an EDLC operated with 1 M  $\text{TEABF}_4/\text{ACN}$  organic electrolyte and Ketjen black electrodes. Carbonized PIL fibers (cPF) were used as the current collector.

band is associated with structural defects or disordered graphite, the G-band indicates the presence of  $\text{sp}^2$ -bonded carbon, and the intensity ratio between them,  $I_D/I_G$ , is commonly attributed to the level of carbon ordering. The XRD and Raman patterns of the cPF and PAN-NF indicate comparable degrees of graphitization. The nitrogen contents in the PIL- and PAN-derived carbon materials are also comparable, in between 8 and 9 wt % (Table S2). Thus, the difference in conductivity and EDLC performance could be either a result of the ionic character of the PIL precursor of the cPF or a result of differences in the textures of the carbonized

fibers such as their density, diameter, and densities of interconnections. The higher intrinsic porosity of cPFs can also provide more contact area with the carbon electrodes, thus lowering the contact resistance and providing higher rate capability, in agreement with impedance spectroscopy measurements (Figure S6). To test the compatibility of cPF with different electrodes, cPF was used in a supercapacitor with a self-made hard-salt-templated carbon (HSTC) electrode. Again, its performance nearly matches that of Pt-f (Figure 5), verifying that it could be used in combination with different electrodes.

cPF was also tested in an organic EDLC operated with 1 M tetraethylammonium tetrafluoroborate/acetonitrile (TEABF<sub>4</sub>/ACN) solution and with Ketjen black carbon as the electrode material, presenting remarkable performance in this electrolyte, too. The nearly rectangular shape in CV curves shows good EDLC performance (Figure 6a). No notable loss of capacitance was observed in a floating test with potential hold at 2.5 V for 100 h, indicating the absence of degradation of the used CC (Figure 6b). The high capacitance retention at high current densities (Figure 6c), which seemed not to be limited by the use of cPF CC, and the low resistance in the impedance spectra (Figure 6d) further indicate that the cPF allows for high rates.

The weight of cPF is significantly lighter than the corresponding carbon-coated aluminum. Usually, aluminum foils with a thickness of 20–80 μm are used as CCs.<sup>77,78</sup> Taking into account a density of 2.7 g cm<sup>-3</sup>, and neglecting the weight of the carbon coating, a disc-shaped sample with a diameter of 1 cm would weight 4.2–16.9 mg. A similar sample of cPF weighed 0.2–0.4 mg, leading to a decrease of 90–98% in the CC weight. The reduced weight of the CC provides the opportunity to fabricate lighter devices.

## CONCLUSIONS

An all-carbon fibrous current collector with electrospun PIL as the carbon precursor was developed. The free-standing conductive carbon has been produced with the use of electrospinning, which allowed for the creation of sub-micrometer interconnected fibers. For the first time, it has been possible to retain the fiber structure of PIL upon carbonization due to postspinning cross-linking. This was accomplished by first incorporating a polyvalent organic acid in the spinning solution followed by ammonia treatment, which deprotonated the carboxylic acid units and activated the cross-linking process. This key step led to retainment of the material's structure during carbonization at 950 °C to produce carbon fibers. cPF were applied as current collectors in EDLCs based on aqueous and organic electrolytes and with different active electrode materials. They operated at current densities of up to 40 A g<sup>-1</sup> without significant loss of capacity, thus outperforming established carbon-coated aluminum foil and demonstrating capabilities similar to platinum, with good stability and low resistance. The mechanical stability and processability of the carbonized fibers are high enough to engineer them into EDLC devices without macroscopic damage; more work is to be done to accommodate these fibers in flexible devices.<sup>79</sup> PIL-derived carbon fibers could also have potential as hosts for guest species; carbon fibers have been used for deposition of various materials,<sup>80</sup> such as LaB<sub>6</sub> nanowires on carbon fiber cloth<sup>81</sup> and electrospinning of PAN with iron oxide.<sup>82</sup> Although this technology is still far from commercialization due to the high price of PILs, the scalability of the production method together with the high conductivity and low weight of the carbon fleece establish the potential of PIL-derived carbon fibers as a metal-free alternative for future EDLC application.

## MATERIALS AND METHODS

**Materials.** Polyvinylpyrrolidone (PVP, 1.3 MDa), 1-vinylimidazole, and bromoacetonitrile were supplied from Alfa Aesar. All solvents were analytical grade and supplied from Merck: dimethylformamide (DMF), methanol, dimethyl sulfoxide (DMSO), acetone, acetonitrile (ACN), and diethyl ether. Other chemicals were

bis(trifluoromethane)sulfonimide lithium salt (LiTFSI) (io-li-tech), benzenepentacarboxylic acid (BPC) (TCI Chemicals), terephthalic acid (Aldrich), polyacrylonitrile (150 kDa, Aldrich), oxalic acid (OA) (Fluka), and butylated hydroxytoluene. All materials were used as received except azobis(isobutyronitrile) (AIBN), which was recrystallized in methanol.

**Polymer Synthesis.** The synthesis of PIL was performed according to a previously described procedure.<sup>60</sup> Details of the reaction can be found in the Supporting Information (<sup>1</sup>H NMR spectrum in Figure S7). The chemical structures of PIL, BPC, and OA are depicted in Figure S8.

**Preparation of PIL-Derived Carbons.** To prepare the spinning solutions, PIL (20 wt %) and PVP (5 wt %) were mixed with DMF:methanol 25:75 (w:w) using a magnetic stirrer heated to 35 °C. OA (1.4 wt %) and BPC (0.7 wt %) were added to the spinning solution at a concentration that corresponds to a molar ratio of 0.6 and 0.25 between COOH groups and PIL repeating unit, respectively. Solutions were transferred to a 2 mL syringe and mounted on the syringe pump in a spinning machine (Professional Electrospinner, Yflow, Spain). A positive high voltage was connected via alligator clip to a needle with an inner diameter of 0.5 mm and an outer diameter of 1 mm. The collecting plate was covered with aluminum foil and connected to a ground. Process parameters were fixed at a voltage of 20 kV, flow rate of 1.2 mL h<sup>-1</sup>, and distance from tip to collector of 10 cm. The temperature was 23 °C, and the humidity was 40–50%. The spun sheets were submerged for 2 h in an aqueous ammonia solution (0.06 vol % ammonium hydroxide). The sheets were then placed between two stainless steel meshes with a weight on top to keep the sheets flat and dried in air overnight. For carbonization, sheets were placed in a porcelain dish, heated in a chamber furnace to the desired temperature under flow of N<sub>2</sub> at a heating rate of 10 K min<sup>-1</sup>, and held in the desired temperature for 1 h. SEM micrograph of the cross section revealed an average thickness of 10–15 μm (Figure S9a).

To prepare PIL-derived carbon film (PIL-film), a solution similar to the spinning solution but half in solid content was casted to a Petri dish and air-dried. It was then cross-linked and carbonized under the same conditions as PIL fibers. The thickness was estimated to be 80–90 μm by using SEM (Figure S9b).

**Preparation of PAN Fibers.** PAN-derived carbon fibers (PAN-NF) were prepared by electrospinning PAN (10 wt %) in DMF using a flow rate of 4 mL h<sup>-1</sup>, a distance of 18 cm, and a voltage of 15.4 kV. Fibers were air stabilized by heating at a 225 K h<sup>-1</sup> rate to 250 °C and holding for 0.5 h, followed by carbonization under nitrogen flow at a heating rate of 10 K min<sup>-1</sup> to 950 °C and holding for 1 h. The thickness was estimated to be 10–15 μm by using SEM (Figure S9c). SEM micrographs of PAN fibers after carbonization can be found in Figure S1b.

**Characterization.** Thermogravimetric analysis (TGA) measurements were conducted using a thermo-microbalance TG 209 F1 Libra (Netzsch, Selb, Germany) with a heating rate of 10 K min<sup>-1</sup> under nitrogen flow. SEM was performed on a GEMINI LEO 1550 microscope at 3 kV; samples were coated with a thin layer of gold and palladium before examination. GPC was performed at 25 °C in a NOVEMA Max linear S column using an eluent of 80% aqueous acetate buffer and 20% methanol (flow rate 1.00 mL min<sup>-1</sup>, pullulan standards), connected to a Shodex refractive index detector RI-101.

Elemental analysis was performed with a vario MICRO cube CHNOS elemental analyzer (Elementar Analysensysteme GmbH, Langenselbold) in the CHNS mode. The N<sub>2</sub> physisorption experiment was performed at 77 K on a Quadrasorb apparatus from Quantachrome Instruments. Samples were outgassed at 150 °C for 20 h under vacuum prior to the measurement. The specific surface area was calculated by using the multipoint Brunauer–Emmett–Teller (BET) model ( $p/p_0 = 0.05–0.2$ ). Pore size distributions were calculated by using the quenched-solid density functional theory (QSDFT) method (adsorption branch kernel) for N<sub>2</sub> adsorbed on carbon with a slit/cylindrical pore shape at 77 K. X-ray diffraction (XRD) patterns were recorded on a Bruker D8 ADVANCE X-ray diffractometer with Cu K $\alpha$  radiation and Sol-X detector and were background-subtracted and smoothed by using Match! software. The

carbon fiber samples were grinded in a mortar before the measurements. Raman spectra were obtained by using a Renishaw inVia Raman microscope operating with an objective (Nikon, 10×/0.25, ∞/− WD 6.1) and an excitation wavelength of 532 nm with a power of 4.0 mW. The sheet resistance was measured by using a four-point probe (Keithley 2400); the reported resistances are an average of at least four measurements.<sup>83</sup>

**Electrical Double-Layer Capacitor Assembly.** Free-standing electrodes for EDLCs were fabricated by mixing carbon materials (Ketjen black or HSTC<sup>9</sup>) and polytetrafluoroethylene (PTFE, 60 wt % solution in H<sub>2</sub>O from Sigma-Aldrich) with a mass ratio of ~9:1 in ethanol. The solution was then poured on a glass plate and mixed with razor blades until it changed to a rubber-like consistency. Afterward, it was placed into aluminum foil and rolled to thin sheets (thicknesses 180 ± 10 μm) using a commercial roll mill, followed by punching into free-standing electrode disks of 10 mm in diameter. The areal loading of active material on an electrode was about 5 mg cm<sup>-2</sup>. The electrodes were dried at 60 °C for 12 h under air. EDLCs were tested with a symmetrical two-electrode configuration employing 1 M Na<sub>2</sub>SO<sub>4</sub> aqueous solution, or 1 M tetraethylammonium tetrafluoroborate/acetonitrile solution (TEABF<sub>4</sub>/ACN) as the electrolytes. Typically, a custom-built cell (with a spring to control the pressure at 10 MPa and highly conductive titanium pistons) was assembled by using a pair of circular electrodes sandwiching a separator, with electrolytes (80 μL), and two pieces of the as-prepared carbon nanofibers as the current collectors.<sup>84</sup> To emphasize the merits of the PIL NF current collector, the platinum foils (120 μm thick, Alfa Aesar) and carbon-coated Al foils (16 μm thick, Shanghai Jima Industrial Co., Limited) were employed as the reference current collectors. A Dreamweaver Silver (Dreamweaver International Inc.) separator of 13 mm in diameter was used for the aqueous electrolyte, while a 25 μm trilayer polypropylene–polyethylene–polypropylene membrane (Celgard 2325, 13 mm in diameter) was used as separator in TEABF<sub>4</sub>/AN electrolyte. For the aqueous electrolyte, the device assembly took place under an air atmosphere. For the organic electrolyte, EDLCs were assembled in an argon-filled glovebox (H<sub>2</sub>O < 0.1 ppm, O<sub>2</sub> < 0.1 ppm). A Biologic MPG-2 galvanostat/potentiostat was used for electrochemical characterization. All measurements were performed at room temperature. The electrochemical impedance spectroscopy was performed at open circuit potential with a sinusoidal signal over a frequency range from 20 kHz to 10<sup>-2</sup> Hz at an amplitude of 10 mV.

Cyclic voltammetry (CV) tests were performed at scan rates of 2–500 mV s<sup>-1</sup>. The carbon differential gravimetric capacitance for CV plots, C<sub>d</sub> (F g<sup>-1</sup>), was calculated according to the following equation:

$$C_d = \frac{2I}{m\gamma} \quad (1)$$

where  $I$  is the current (A),  $\gamma$  is the scan rate (V s<sup>-1</sup>), and  $m$  is the active mass in a single carbon electrode (g).

A galvanostatic charge/discharge with potential limitation (GCPL) was applied at specific currents between 0.1 and 40 A g<sup>-1</sup> in different cell voltage ranges (0 to +0.8 V and 0 to +2.5 V for aqueous and organic electrolytes, respectively). The carbon gravimetric capacitance,  $C$  (F g<sup>-1</sup>), was calculated according to the following equation:

$$C = \frac{2Q_{\text{dis}}}{(V - V_{\text{drop}})m} \quad (2)$$

where  $Q_{\text{dis}}$  (C) is the charge of the discharging cycle,  $V$  (V) is the discharging potential change,  $V_{\text{drop}}$  (V) is the voltage drop at the beginning of the discharge, and  $m$  (g) is the active mass in a single carbon electrode.

The stability measurement was performed by the floating test. Typically, the voltage was kept at 2.5 V for 100 h, and the specific capacity was measured every 10 h by galvanostatic cycling at 1 A g<sup>-1</sup>. SEM images after cycling were obtained by assembling cPF (as both current collectors and electrodes) into an EDLC cell and cycling 1000 times at a specific current of 1 A g<sup>-1</sup> by using the aqueous electrolyte.

## ■ ASSOCIATED CONTENT

### 📄 Supporting Information

The Supporting Information is available free of charge on the ACS Publications website at DOI: 10.1021/acsaeam.9b00854.

Detailed synthesis of the PIL, optimization of the cross-linker concentration, <sup>1</sup>H NMR spectrum of the PIL and its structure, SEM micrographs of the cross section and top view of fibers carbonized at 950 °C, TGA of the PIL cross-linked fibers, PIL and PVP; impedance spectroscopy measurements of an EDLC, CV curves with cPF acting as the electrode and current collector, nitrogen physisorption isotherm of cPF and Ketjen black, elemental analysis of electrospun PIL fibers, XRD, Raman and sheet resistance of cPF and carbonized PAN fibers (PDF)

## ■ AUTHOR INFORMATION

### Corresponding Author

\*E-mail Elinor.josef@mpikg.mpg.de.

### ORCID

Elinor Josef: 0000-0002-9744-7399

Ryan Guterman: 0000-0003-3231-6176

### Notes

The authors declare no competing financial interest.

## ■ ACKNOWLEDGMENTS

We thank Dr. Felix Hippauf, Dr. Jonas Pampel, and Dipl.-Ing-Paul Härtel (Fraunhofer IWS Dresden) for the four-point measurements and fruitful discussions. We thank the Max Planck Society for financial support.

## ■ REFERENCES

- Wang, Y.; Song, Y.; Xia, Y. Electrochemical Capacitors: Mechanism, Materials, Systems, Characterization and Applications. *Chem. Soc. Rev.* **2016**, *45*, 5925–5950.
- Simon, P.; Gogotsi, Y. Materials for Electrochemical Capacitors. *Nat. Mater.* **2008**, *7*, 845–854.
- Yan, J.; Wang, Q.; Wei, T.; Fan, Z. Recent Advances in Design and Fabrication of Electrochemical Supercapacitors with High Energy Densities. *Adv. Energy Mater.* **2014**, *4*, 1300816.
- Salanne, M.; Rotenberg, B.; Naoi, K.; Kaneko, K.; Taberna, P.-L.; Grey, C. P.; Dunn, B.; Simon, P. Efficient Storage Mechanisms for Building Better Supercapacitors. *Nat. Energy* **2016**, *1*, 16070.
- Jäckel, N.; Simon, P.; Gogotsi, Y.; Presser, V. Increase in Capacitance by Subnanometer Pores in Carbon. *ACS Energy Lett.* **2016**, *1*, 1262–1265.
- Simon, P.; Gogotsi, Y. Capacitive Energy Storage in Nanostructured Carbon-Electrolyte Systems. *Acc. Chem. Res.* **2013**, *46*, 1094–1103.
- Borchardt, L.; Oschatz, M.; Paasch, S.; Kaskel, S.; Brunner, E. Interaction of Electrolyte Molecules with Carbon Materials of Well-Defined Porosity: Characterization by Solid-State NMR Spectroscopy. *Phys. Chem. Chem. Phys.* **2013**, *15*, 15177.
- Borchardt, L.; Oschatz, M.; Kaskel, S. Tailoring Porosity in Carbon Materials for Supercapacitor Applications. *Mater. Horiz.* **2014**, *1*, 157–168.
- Yan, R.; Heil, T.; Presser, V.; Walczak, R.; Antonietti, M.; Oschatz, M. Ordered Mesoporous Carbons with High Micropore Content and Tunable Structure Prepared by Combined Hard and Salt Templating as Electrode Materials in Electric Double-Layer Capacitors. *Adv. Sustain. Syst.* **2018**, *2*, 1700128.
- Bo, Z.; Zhu, W.; Ma, W.; Wen, Z.; Shuai, X.; Chen, J.; Yan, J.; Wang, Z.; Cen, K.; Feng, X. Vertically Oriented Graphene Bridging

Active-Layer/Current-Collector Interface for Ultrahigh Rate Supercapacitors. *Adv. Mater.* **2013**, *25*, 5799–5806.

(11) Zhou, R.; Meng, C.; Zhu, F.; Li, Q.; Liu, C.; Fan, S.; Jiang, K. High-Performance Supercapacitors Using a Nanoporous Current Collector Made from Super-Aligned Carbon Nanotubes. *Nanotechnology* **2010**, *21*, 345701.

(12) Huang, Y.; Li, Y.; Gong, Q.; Zhao, G.; Zheng, P.; Bai, J.; Gan, J.; Zhao, M.; Shao, Y.; Wang, D.; et al. Hierarchically Mesoporous Aluminum Current Collector for Enhancing the Performance of Supercapacitors. *ACS Appl. Mater. Interfaces* **2018**, *10*, 16572–16580.

(13) Mehrabi-Matin, B.; Shahrokhian, S.; Iraj-Zad, A. Silver Fiber Fabric as the Current Collector for Preparation of Graphene-Based Supercapacitors. *Electrochim. Acta* **2017**, *227*, 246–254.

(14) Randolfo, A. G.; Hollenkamp, A. F. Carbon Properties and Their Role in Supercapacitors. *J. Power Sources* **2006**, *157*, 11–27.

(15) Blomquist, N.; Wells, T.; Andres, B.; Bäckström, J.; Forsberg, S.; Olin, H. Metal-Free Supercapacitor with Aqueous Electrolyte and Low-Cost Carbon Materials. *Sci. Rep.* **2017**, *7*, 1–7.

(16) Vilatela, J. J.; Marcella, R. Tough Electrodes: Carbon Nanotube Fibers as the Ultimate Current Collectors/Active Material for Energy Management Devices. *Chem. Mater.* **2015**, *27*, 6901–6917.

(17) Pourjavadi, A.; Doroudian, M.; Ahadpour, A.; Pourbadie, B. Preparation of Flexible and Free-Standing Graphene-Based Current Collector via a New and Facile Self-Assembly Approach: Leading to a High Performance Porous Graphene/Polyaniline Supercapacitor. *Energy* **2018**, *152*, 178–189.

(18) Miao, F.; Shao, C.; Li, X.; Lu, N.; Wang, K.; Zhang, X.; Liu, Y. Polyaniline-Coated Electrospun Carbon Nanofibers with High Mass Loading and Enhanced Capacitive Performance as Freestanding Electrodes for Flexible Solid-State Supercapacitors. *Energy* **2016**, *95*, 233–241.

(19) Quintero, R.; Kim, D. Y.; Hasegawa, K.; Yamada, Y.; Yamada, A.; Noda, S. Carbon Nanotube 3D Current Collectors for Lightweight, High Performance and Low Cost Supercapacitor Electrodes. *RSC Adv.* **2014**, *4*, 8230.

(20) Kaempgen, M.; Chan, C. K.; Ma, J.; Cui, Y.; Gruner, G. Printable Thin Film Supercapacitors Using Single-Walled Carbon Nanotubes. *Nano Lett.* **2009**, *9*, 1872–1876.

(21) Niu, Z.; Zhou, W.; Chen, J.; Feng, G.; Li, H.; Ma, W.; Li, J.; Dong, H.; Ren, Y.; Zhao, D.; et al. Compact-Designed Supercapacitors Using Free-Standing Single-Walled Carbon Nanotube Films. *Energy Environ. Sci.* **2011**, *4*, 1440–1446.

(22) Hu, L.; Wu, H.; La Mantia, F.; Yang, Y.; Cui, Y. Thin, Flexible Secondary Li-Ion Paper Batteries. *ACS Nano* **2010**, *4*, 5843–5848.

(23) Narubayashi, M.; Chen, Z.; Hasegawa, K.; Noda, S. 50–100 Mm-Thick Pseudocapacitive Electrodes of MnO<sub>2</sub>nanoparticles Uniformly Electrodeposited in Carbon Nanotube Papers. *RSC Adv.* **2016**, *6*, 41496–41505.

(24) Liu, J.; Mirri, F.; Notarianni, M.; Pasquali, M.; Motta, N. High Performance All-Carbon Thin Film Supercapacitors. *J. Power Sources* **2015**, *274*, 823–830.

(25) Notarianni, M.; Liu, J.; Mirri, F.; Pasquali, M.; Motta, N. Graphene-Based Supercapacitor with Carbon Nanotube Film as Highly Efficient Current Collector. *Nanotechnology* **2014**, *25*, 435405.

(26) Horng, Y. Y.; Lu, Y. C.; Hsu, Y. K.; Chen, C. C.; Chen, L. C.; Chen, K. H. Flexible Supercapacitor Based on Polyaniline Nanowires/Carbon Cloth with Both High Gravimetric and Area-Normalized Capacitance. *J. Power Sources* **2010**, *195*, 4418–4422.

(27) Liu, X.; Naylor Marlow, M.; Cooper, S. J.; Song, B.; Chen, X.; Brandon, N. P.; Wu, B. Flexible All-Fiber Electrospun Supercapacitor. *J. Power Sources* **2018**, *384*, 264–269.

(28) Marthia, S. K.; Dudney, N. J.; Kiggans, J. O.; Nanda, J. Electrochemical Stability of Carbon Fibers Compared to Aluminum as Current Collectors for Lithium-Ion Batteries. *J. Electrochem. Soc.* **2012**, *159*, A1652–A1658.

(29) Lu, X.; Wang, C.; Wei, Y. One-Dimensional Composite Nanomaterials: Synthesis by Electrospinning and Their Applications. *Small* **2009**, *5*, 2349–2370.

(30) Inagaki, M.; Yang, Y.; Kang, F. Carbon Nanofibers Prepared via Electrospinning. *Adv. Mater.* **2012**, *24*, 2547–2566.

(31) Kenry; Lim, C. T. Nanofiber Technology: Current Status and Emerging Developments. *Prog. Polym. Sci.* **2017**, *70*, 1–17.

(32) Feng, L.; Xie, N.; Zhong, J. Carbon Nanofibers and Their Composites: A Review of Synthesizing, Properties and Applications. *Materials* **2014**, *7*, 3919–3945.

(33) Presser, V.; Zhang, L.; Niu, J. J.; McDonough, J.; Perez, C.; Fong, H.; Gogotsi, Y. Flexible Nano-Felts of Carbide-Derived Carbon with Ultra-High Power Handling Capability. *Adv. Energy Mater.* **2011**, *1*, 423–430.

(34) Tolosa, A.; Krüner, B.; Jäckel, N.; Aslan, M.; Vakifahmetoglu, C.; Presser, V. Electrospinning and Electrospinning of Silicon Oxycarbide-Derived Nanoporous Carbon for Supercapacitor Electrodes. *J. Power Sources* **2016**, *313*, 178–188.

(35) Lu, X.; Wang, C.; Favier, F.; Pinna, N. Electrospun Nanomaterials for Supercapacitor Electrodes: Designed Architectures and Electrochemical Performance. *Adv. Energy Mater.* **2017**, *7*, 1601301.

(36) Xu, H.; Hu, X.; Yang, H.; Sun, Y.; Hu, C.; Huang, Y. Flexible Asymmetric Micro-Supercapacitors Based on Bi<sub>2</sub>O<sub>3</sub> and MnO<sub>2</sub> Nanoflowers: Larger Areal Mass Promises Higher Energy Density. *Adv. Energy Mater.* **2015**, *5*, 1401882.

(37) Mao, X.; Hatton, T.; Rutledge, G. A Review of Electrospun Carbon Fibers as Electrode Materials for Energy Storage. *Curr. Org. Chem.* **2013**, *17*, 1390–1401.

(38) Kim, B. H.; Bui, N.-N.; Yang, K.-S.; dela Cruz, M. E. D.; Ferraris, J. P. Electrochemical Properties of Activated Polyacrylonitrile/Pitch Carbon Fibers Produced Using Electrospinning. *Bull. Korean Chem. Soc.* **2009**, *30*, 1967–1972.

(39) Guo, Q.; Zhou, X.; Li, X.; Chen, S.; Seema, A.; Greiner, A.; Hou, H. Supercapacitors Based on Hybrid Carbon Nanofibers Containing Multiwalled Carbon Nanotubes. *J. Mater. Chem.* **2009**, *19*, 2810.

(40) Wei, M.; Jiang, M.; Liu, X.; Wang, M.; Mu, S. Graphene-Doped Electrospun Nanofiber Membrane Electrodes and Proton Exchange Membrane Fuel Cell Performance. *J. Power Sources* **2016**, *327*, 384–393.

(41) Chee, W. K.; Lim, H. N.; Zainal, Z.; Harrison, I.; Andou, Y.; Huang, N. M.; Altarawneh, M.; Jiang, Z. T. Electrospun Graphene Nanoplatelets-Reinforced Carbon Nanofibers as Potential Supercapacitor Electrode. *Mater. Lett.* **2017**, *199*, 200–203.

(42) Ekabutr, P.; Ariyathanakul, T.; Chaiyo, S.; Niamlang, P.; Rattanaveeranon, S.; Chailapakul, O.; Supaphol, P. Carbonized Electrospun Polyvinylpyrrolidone/Metal Hybrid Nanofiber Composites for Electrochemical Applications. *J. Appl. Polym. Sci.* **2018**, *135*, 45639.

(43) Qian, W.; Texter, J.; Yan, F. Frontiers in Poly(Ionic Liquid)s: Syntheses and Applications. *Chem. Soc. Rev.* **2017**, *46*, 1124–1159.

(44) Ajjan, F. N.; Ambrogio, M.; Tiruye, G. A.; Cordella, D.; Fernandes, A. M.; Grygiel, K.; Isik, M.; Patil, N.; Porcarelli, L.; Rocasalbas, G.; et al. Innovative Polyelectrolytes/Poly(Ionic Liquid)s for Energy and the Environment. *Polym. Int.* **2017**, *66*, 1119–1128.

(45) Mecerreyes, D. Polymeric Ionic Liquids: Broadening the Properties and Applications of Polyelectrolytes. *Prog. Polym. Sci.* **2011**, *36*, 1629–1648.

(46) Yuan, J.; Mecerreyes, D.; Antonietti, M. Poly(Ionic Liquid)s: An Update. *Prog. Polym. Sci.* **2013**, *38*, 1009–1036.

(47) Bara, J. E.; Camper, D. E.; Gin, D. L.; Noble, R. D. Room-Temperature Ionic Liquids and Composite Materials: Platform Technologies for CO<sub>2</sub> Capture. *Acc. Chem. Res.* **2010**, *43*, 152–159.

(48) Jangu, C.; Long, T. E. Phosphonium Cation-Containing Polymers: From Ionic Liquids to Polyelectrolytes. *Polymer* **2014**, *55*, 3298–3304.

(49) Yuan, J.; Giordano, C.; Antonietti, M. Ionic Liquid Monomers and Polymers as Precursors of Highly Conductive, Mesoporous, Graphitic Carbon Nanostructures. *Chem. Mater.* **2010**, *22*, 5003–5012.

- (50) Yuan, J.; Márquez, A. G.; Reinacher, J.; Giordano, C.; Janek, J.; Antonietti, M. Nitrogen-Doped Carbon Fibers and Membranes by Carbonization of Electrospun Poly(Ionic Liquid)S. *Polym. Chem.* **2011**, *2*, 1654–1657.
- (51) Xie, Z. L.; Su, D. S. Ionic Liquid Based Approaches to Carbon Materials Synthesis. *Eur. J. Inorg. Chem.* **2015**, *2015*, 1137–1147.
- (52) Fellingner, T.-P.; Thomas, A.; Yuan, J.; Antonietti, M. 25th Anniversary Article: “Cooking Carbon with Salt”: Carbon Materials and Carbonaceous Frameworks from Ionic Liquids and Poly(Ionic Liquid)S. *Adv. Mater.* **2013**, *25*, 5838–5855.
- (53) Paraknowitsch, J. P.; Thomas, A. Doping Carbons beyond Nitrogen: An Overview of Advanced Heteroatom Doped Carbons with Boron, Sulphur and Phosphorus for Energy Applications. *Energy Environ. Sci.* **2013**, *6*, 2839–2855.
- (54) Podyacheva, O. Y.; Cherepanova, S. V.; Romanenko, A. I.; Kibis, L. S.; Svintsitskiy, D. A.; Boronin, A. I.; Stonkus, O. A.; Suboch, A. N.; Puzynin, A. V.; Ismagilov, Z. R. Nitrogen Doped Carbon Nanotubes and Nanofibers: Composition, Structure, Electrical Conductivity and Capacity Properties. *Carbon* **2017**, *122*, 475–483.
- (55) McKee, M. G.; Hunley, M. T.; Layman, J. M.; Long, T. E. Solution Rheological Behavior and Electrospinning of Cationic Polyelectrolytes. *Macromolecules* **2006**, *39*, 575–583.
- (56) Einert, M.; Wessel, C.; Badaczewski, F.; Leichtweiß, T.; Eufinger, C.; Janek, J.; Yuan, J.; Antonietti, M.; Smarsly, B. M.; Eufi, C.; et al. Nitrogen-Doped Carbon Electrodes: Influence of Microstructure and Nitrogen Configuration on the Electrical Conductivity of Carbonized Polyacrylonitrile and Poly(Ionic Liquid) Blends. *Macromol. Chem. Phys.* **2015**, *216*, 1930–1944.
- (57) Chen, H.; Elabd, Y. A. Polymerized Ionic Liquids: Solution Properties and Electrospinning. *Macromolecules* **2009**, *42*, 3368–3373.
- (58) Pang, H.-W.; Yu, H.-F.; Huang, Y.-J.; Li, C.-T.; Ho, K.-C. Electrospun Membranes of Imidazole-Grafted PVDF-HFP Polymeric Ionic Liquids for Highly Efficient Quasi-Solid-State Dye-Sensitized Solar Cells. *J. Mater. Chem. A* **2018**, *6*, 14215–14223.
- (59) Montolio, S.; Abarca, G.; Porcar, R.; Dupont, J.; Burguete, M. I.; García-Verdugo, E.; Luis, S. V. Hierarchically Structured Polymeric Ionic Liquids and Polyvinylpyrrolidone Mat-Fibers Fabricated by Electrospinning. *J. Mater. Chem. A* **2017**, *5*, 9733–9744.
- (60) Zhao, Q.; Fellingner, T.-P.; Antonietti, M.; Yuan, J. A Novel Polymeric Precursor for Micro/Mesoporous Nitrogen-Doped Carbons. *J. Mater. Chem. A* **2013**, *1*, 5113.
- (61) Inagaki, M.; Kang, F.; Toyoda, M.; Konno, H. Carbon Nanofibers Via Electrospinning. *Adv. Mater. Sci. Eng. Carbon* **2014**, *4*, 165–188.
- (62) Täuber, K.; Dani, A.; Yuan, J. Covalent Cross-Linking of Porous Poly(Ionic Liquid) Membrane via a Triazine Network. *ACS Macro Lett.* **2017**, *6*, 1–5.
- (63) Soll, S.; Zhao, Q.; Weber, J.; Yuan, J. Activated CO<sub>2</sub> Sorption in Mesoporous Imidazolium-Type Poly(Ionic Liquid)-Based Polyampholytes. *Chem. Mater.* **2013**, *25*, 3003–3010.
- (64) Zhao, Q.; Soll, S.; Antonietti, M.; Yuan, J. Organic Acids Can Crosslink Poly(Ionic Liquid)s into Mesoporous Polyelectrolyte Complexes. *Polym. Chem.* **2013**, *4*, 2432.
- (65) Tauber, K.; Zhao, Q.; Antonietti, M.; Yuan, J. Tuning the Pore Size in Gradient Poly(Ionic Liquid) Membranes by Small Organic Acids. *ACS Macro Lett.* **2015**, *4*, 39–42.
- (66) Chen, Y.; Feng, H.; Wang, Y.; Tang, Z.; Chua, D. Nano-Porous Copper Metal Current Collector for Lithium Ion Batteries. *Mater. Lett.* **2018**, *226*, 8–12.
- (67) Arjmand, M.; Chizari, K.; Krause, B.; Pötschke, P.; Sundararaj, U. Effect of Synthesis Catalyst on Structure of Nitrogen-Doped Carbon Nanotubes and Electrical Conductivity and Electromagnetic Interference Shielding of Their Polymeric Nanocomposites. *Carbon* **2016**, *98*, 358–372.
- (68) Eftekhari, A. The Mechanism of Ultrafast Supercapacitors. *J. Mater. Chem. A* **2018**, *6*, 2866–2876.
- (69) Yoo, Y.; Park, J.; Kim, M.-S.; Kim, W. Development of 2.8 V Ketjen Black Supercapacitors with High Rate Capabilities for AC Line Filtering. *J. Power Sources* **2017**, *360*, 383–390.
- (70) Peng, T.; Zhao, T.; Zhou, Q.; Zhou, H.; Wang, J.; Liu, J.; Liu, Q. Design of Mass-Controllable NiCo<sub>2</sub>S<sub>4</sub>/Ketjen Black Nanocomposite Electrodes for High Performance Supercapacitors. *CrystEngComm* **2015**, *17*, 7583–7591.
- (71) Oschatz, M.; Boukhalfa, S.; Nickel, W.; Hofmann, J. P.; Fischer, C.; Yushin, G.; Kaskel, S. Carbide-Derived Carbon Aerogels with Tunable Pore Structure as Versatile Electrode Material in High Power Supercapacitors. *Carbon* **2017**, *113*, 283–291.
- (72) Zhang, X.; Jiao, Y.; Sun, L.; Wang, L.; Wu, A.; Yan, H.; Meng, M.; Tian, C.; Jiang, B.; Fu, H. GO-Induced Assembly of Gelatin toward Stacked Layer-like Porous Carbon for Advanced Supercapacitors. *Nanoscale* **2016**, *8*, 2418–2427.
- (73) Zhao, J.; Jiang, Y.; Fan, H.; Liu, M.; Zhuo, O.; Wang, X.; Wu, Q.; Yang, L.; Ma, Y.; Hu, Z. Porous 3D Few-Layer Graphene-like Carbon for Ultrahigh-Power Supercapacitors with Well-Defined Structure-Performance Relationship. *Adv. Mater.* **2017**, *29*, 1604569.
- (74) Wu, M.; Wang, Q.; Li, K.; Wu, Y.; Liu, H. Optimization of Stabilization Conditions for Electrospun Polyacrylonitrile Nanofibers. *Polym. Degrad. Stab.* **2012**, *97*, 1511–1519.
- (75) Kim, C.; Park, S. H.; Cho, J. I.; Lee, D. Y.; Park, T. J.; Lee, W. J.; Yang, K. S. Raman Spectroscopic Evaluation of Polyacrylonitrile-Based Carbon Nanofibers Prepared by Electrospinning. *J. Raman Spectrosc.* **2004**, *35*, 928–933.
- (76) Ji, L.; Zhang, X. Electrospun Carbon Nanofibers Containing Silicon Particles as an Energy-Storage Medium. *Carbon* **2009**, *47*, 3219–3226.
- (77) Burke, A. Ultracapacitors: Why, How, and Where Is the Technology. *J. Power Sources* **2000**, *91*, 37–50.
- (78) Yu, A.; Chabot, V.; Zhang, J. *Electrochemical Supercapacitors for Energy Storage and Delivery*; CRC Press: Boca Raton, FL, 2017.
- (79) Li, H.; Tang, Z.; Liu, Z.; Zhi, C. Evaluating Flexibility and Wearability of Flexible Energy Storage Devices. *Joule* **2019**, *3*, 613–619.
- (80) Xie, S.; Liu, S.; Cheng, P. F.; Lu, X. Recent Advances toward Achieving High-Performance Carbon-Fiber Materials for Supercapacitors. *ChemElectroChem* **2018**, *5*, 571–582.
- (81) Xue, Q.; Tian, Y.; Deng, S.; Huang, Y.; Zhu, M.; Pei, Z.; Li, H.; Liu, F.; Zhi, C. LaB<sub>6</sub> Nanowires for Supercapacitors. *Mater. Today Energy* **2018**, *10*, 28–33.
- (82) Abe, J.; Kawase, K.; Tachikawa, N.; Katayama, Y.; Shiratori, S. Influence of Carbonization Temperature and Press Processing on the Electrochemical Characteristics of Self-Standing Iron Oxide/Carbon Composite Electrospun Nanofibers. *RSC Adv.* **2017**, *7*, 32812–32818.
- (83) Smits, F. M. Measurement of Sheet Resistivities with the Four-Point Probe. *Bell Syst. Technol. J.* **1958**, *37*, 711–718.
- (84) Weingarh, D.; Zeiger, M.; Jäckel, N.; Aslan, M.; Feng, G.; Presser, V. Graphitization as a Universal Tool to Tailor the Potential-Dependent Capacitance of Carbon Supercapacitors. *Adv. Energy Mater.* **2014**, *4*, 1400316.